Zeolite Nanocrystals Inside Mesoporous TUD-1: A High-Performance Catalytic Composite

Peter Waller,[a] Zhiping Shan,[b] Leonardo Marchese,[c] Guiseppina Tartaglione,[c] Wuzong Zhou,[d] Jacobus C. Jansen,*[a] and Thomas Maschmeyer*[e]

Abstract: A hierarchically structured composite material with interconnecting meso- and micropores has been developed with the aim to optimize zeolite performance. A general synthetic method has been developed that, in a controlled manner, allows for various types of nanosized zeolite to be incorporated into a three-dimensional mesoporous matrix. Nanosized zeolite Beta was used to exemplify this new approach, resulting in a system in which zeolite Beta shows a higher cracking activity per gram of zeolite than pure nanosized zeolite Beta for the model feed *n*-hexane. Additionally, FTIR studies of CO and NH_3 adsorption revealed that the nature of the acid sites in the nanozeolite has been partially modified due to the interactions with the mesoporous matrix, TUD-1.

Keywords: heterogeneous catalysis · materials science · mesoporous materials · microporous materials · vibrational spectroscopy · zeolites

Introduction

Zeolites with their uniform micropores are widely employed in industrial catalysis, although the optimization of their performance, due to their low intracrystalline diffusion coefficient, is still an inherent challenge for chemists and chemical engineers.[1] One way to overcome the mass transport limitations is to reduce the zeolite crystals to nanometer size, so that the diffusion path is relatively short and the accessibility of the catalytic sites through the external surface is high.[2] However, nanosized zeolites cannot be used directly, in part, due to their intrinsically poor stability and to the much higher pressure drops in packed-bed reactors (relative to those obtained with conventional catalysts). Therefore, nanozeolites need to be dispersed and stabilized in a porous matrix.

Conventionally zeolites are mixed with a binder and subsequently extruded into beads or pellets, important especially for applications in the petrochemical industry. However, binders are usually not designed and structured for optimal mass transport in terms of high specific surface areas and pore geometry. Generally these kinds of composite catalysts possess macro-, meso-, and micropores with total Brunauer–Emmet–Teller (BET) surface areas of only around 300 m^2g^{-1}.

Alternative approaches reported are: coating of zeolites on alumina (with BET surface areas depending mainly one the alumina used, that is, ~300 m^2g^{-1}) and shaping of zeolite crystallites into macroporous aggregates, which leads to materials with macropore walls built of zeolites (BET surface areas of 300–400 m^2g^{-1}).[5–6] The in-situ synthesis of small zeolite crystals inside or outside porous silica gel[3] or carbon[4] has also been reported. However, the crystal properties, such as composition, size, and morphology, could not be controlled, because of the bimodal pore structure of the silica gel employed (average pore diameters of 25 and 1000 nm): depending on the pore diameter, crystals with diameters from 20–900 nm were found, largely blocking the porous host.

To prepare catalysts of nanosized zeolites, recently developed mesoporous materials, for example, MCM-41,[7] MUS-x,[8] and SBA-n,[9] are more suitable supports or intergrowth

[a] Dr. P. Waller, Dr. J. C. Jansen
Ceramic Membrane Centre, "The Pore"
Julianalaan 136, 2628 BL Delft (The Netherlands)
Fax: (+31) 15-278-4289
E-mail: J.C.Jansen@tnw.tudelft.nl

[b] Dr. Z. Shan
ABB-Lummus Global Inc.
1515 Broad Street, Bloomfield, NJ 07003-3096 (USA)

[c] Prof. L. Marchese, Dr. G. Tartaglione
Dipartimento di Scienze e Technologie Avanzate
Universitá del Piemonte Orientale "Amedeo Avogadro"
c.so Borsalino 54, 15100 Alessandria, (Italy)

[d] Dr. W. Zhou
School of Chemistry
University of St. Andrews, KY16 9ST, Fife (Scotland)

[e] Prof. T. Maschmeyer
Centre for Molecular Catalysis
School of Chemistry
The University of Sydney, NSW, 2006, (Australia)
Fax: (+61) 2-9351-3329
E-mail: th.maschmeyer@chem.usyd.edu.au

  DOI: 10.1002/chem.200400343

matrices, due to their high surface areas and their uniform mesopores. Especially SBA-15[9] and TUD-1[10] are attractive, the latter with tunable 3 to 25 nm pores and surface areas of 600 to 1000 m^2g^{-1}. Two principle attempts have been reported regarding the preparation of composites with mesoporous materials: in the first approach, structured mesoporous materials, for example, the M41S family, were used as silica source from which to synthesize the zeolite, for example, FAU[11] or MFI,[12] by partial recrystallization of the mesopore walls. Generally, the zeolite synthesis needs relatively severe conditions in terms of temperature and pH, relative to those employed during the formation of mesoporous materials. Unless extreme fine-tuning of the synthesis composition and concurrent depression of the zeolite growth is applied, the integrity of the metastable mesoporous phase is lost. In the second approach, syntheses have been investigated in which highly ordered mesoporous structures have been generated by means of the self-assembly of pre-formed clusters of zeolite nuclei with surfactant micelles as templates.[13–15] This approach requires clusters of no more than a few nanometers in diameter, or even smaller zeolite nuclei, as a part of building units to form mesoporous structures, since otherwise no well-defined mesostructures are formed. However, these small clusters or nuclei easily loose their integrity during activation through calcination at high temperatures.[16] An issue that is also of potential concern when using zeolite seeds, as reported by Prokesova, et al.[18] Moreover, the physicochemical properties of both the zeolite and the mesoporous materials are difficult to tune independently as the zeolite synthesis is coupled with the mesopore formation.

Our approach is to blend the well-defined, pre-formed zeolite nanocrystallites into the synthesis mixture of the mesoporous carrier. After calcination, a mesoporous matrix is obtained in which individual zeolite crystals are dispersed homogeneously. These zeolite crystallites, diameter 20 to 40 nm, are accessible through the uniform mesopores with tunable diameters of between 3 and 25 nm surrounding the particles; that is, the particles are not buried inaccessibly inside the walls of the mesoporous matrix. Moreover, since the stable and three-dimensional mesoporous material, TUD-1,[10,17] is used as a matrix, mass transfer benefits even more relative to the situation when carrier materials with only one- or two-dimensional pore systems are employed. Here, we describe the key steps to ensure the homogeneity of zeolite particles in the matrix, the structural and vibrational properties of the composite, and the enhancement of cracking activity for the model feed *n*-hexane.

Results and Discussion

Synthesis: Nanosized zeolite crystals (around 40 nm in size) were directly added to the synthesis mixture of TUD-1. To ensure homogeneity of the zeolite crystals in the final mesoporous matrix, a novel but simple synthesis procedure has been established. First, nanosized zeolite particles were homogeneously dispersed in ammonia to avoid the aggregation of zeolite particles. Then the silica source (tetraethylorthosilicate, TEOS) and mesopore template (triethanolamine, TEA) were added under vigorous stirring. To this, a controlled amount of an alkali (tetraethylammonium hydroxide, TEAOH) was added rapidly under stirring and consequently the synthesis mixture became a solid gel. Due to the vigorous stirring, the zeolite particles were homogeneously dispersed in the synthesis mixture before gelation. This homogeneity was maintained during and after gelation due to the sudden and rapid increase of the viscosity in the transition of liquid to thick gel. Under the synthesis conditions applied, the molar ratio of TEAOH/Si <0.1 will favor the gelation, while the ratio >0.2 often leads to a clear solution, causing deposition of zeolite particles.

The solid gel, containing the homogeneous dispersion of zeolite crystals, was aged at room temperature to complete the hydrolysis and polycondensation of the silica source, before being dried at 100 °C to remove water and alcohol (no mesostructure had formed at this stage). Subsequently, the dried gel was heated to 170 °C in an autoclave for 4 h, initiating the formation of mesosized aggregates and eventually shaping the silica phase into a mesoporous structure.[10] After the removal of TEA by calcination, a porous network with interconnecting mesopores and micropores was obtained. The high porosity of the mesoporous matrix ensures a high accessibility to the internal zeolite crystals by external reagents. With this method it is possible to tune the physicochemical properties of both zeolite and mesoporous matrices independently, as they are formed in independent processes.

Integrity of the composite: A typical example of such composites is one that contains different loadings of zeolite Beta (crystal sizes of about 40–50 nm), denoted as Beta-TUD-1. The powder X-ray diffraction patterns are shown in Figure 1

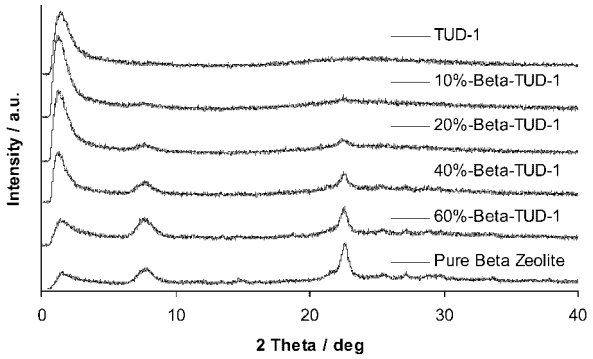

Figure 1. X-ray powder diffraction (XRD) patterns of Beta-TUD-1 containing different amounts of zeolite Beta and pure zeolite Beta.

together with that of the pure zeolite used. Beta-TUD-1 data exhibits the characteristic reflection peaks of zeolite Beta at 7–8.5° and 22.4° in 2θ. In addition, it also shows a peak at about 1.2° in 2θ, characteristic of a mesostructured material. This confirms the co-existence of the zeolite Beta and the mesostructured matrix.

The zeolite loading was estimated from the area under the main peak of zeolite Beta (from 22.0° to 23.0° in 2θ).

The area under the peak from the pure zeolite is taken as 100 wt% zeolite in TUD-1. Figure 2 shows that the calculated composite zeolite loading increases nearly linearly with the loading calculated from the amount of zeolite added to synthesis mixture, indicating that the crystallinity of zeolite Beta is retained after incorporation.

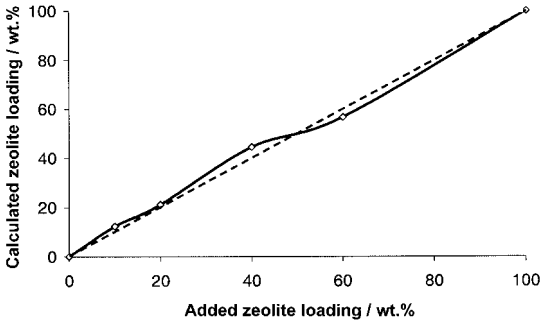

Figure 2. Correlation of the amount of zeolite added with the amount of zeolite in the composite calculated based on XRD pattern peak area.

Meanwhile, it is also clear from Figure 1 and Table 1 that the integrity of the mesostructure decreases with zeolite loading for values above 40%. When the loading reaches 60 wt%, the integrity of the mesostructure is substantially compromised. At lower zeolite loadings (e.g. <40 wt%), the matrix still keeps its high integrity.

Figure 3 shows ^{27}Al NMR spectra of the pure zeolite Beta and Beta-TUD-1 containing 20 and 40 wt% zeolite Beta. No six-coordinate aluminum peak can be observed in Beta-TUD-1, indicating that all aluminum atoms are still four-coordinate (as is the case for aluminum in pure zeolite Beta). Hence, partial dissolution of zeolite crystals during the mesopore formation process and partial structure loss during calcination are not evident, as otherwise some six-coordinate aluminum should be detectable.

Thus, both powder XRD patterns and ^{27}Al NMR spectra of Beta-TUD-1 indicate that the zeolite has been incorporated into the TUD-1 mesoporous matrix and that its structure is retained during the mesopore formation and the calcination processes.

Homogeneity: A TEM image of Beta-TUD-1 (20 wt% zeolite Beta) in Figure 4 clearly shows a three-dimensional sponge- or wormlike mesoporous matrix with some dark gray domains. These domains are estimated to be about 40–50 nm in size, close to that of the original particles added. These domains are larger than the mesopores observed, indicating that the mesoporous matrix surrounds the zeolite particles. The electron diffraction pattern of these domains (inset of Figure 4) gives a *d*-spacing of 1.17 nm, which corresponds to the diffracted beam of the (101) or (011) planes of zeolite Beta. These results indicate that individual nanosized zeolite Beta particles are homogeneously dispersed in the mesoporous host.

When the loading of zeolite increases to 40 wt%, small aggregates (about 80–140 nm) of zeolite crystals start to emerge in the TEM images. However even these small aggregates were homogeneously dispersed in the matrix. Thus, zeolite particles can be 'frozen' into position in the gel network by controlling the gelation of the synthesis mixture.

Table 1. The porosity of Beta-TUD-1 with different Beta zeolite loading, zeolite Beta, and TUD-1.

Sample	S_{BET} [$m^2 g^{-1}$]	t-plot method (de Boer) Surface area [$m^2 g^{-1}$] micropore	mesopore	V_{tp} [$cc\,g^{-1}$]	V_{microp} [$cc\,g^{-1}$]	Average pore diameter [nm] mesopore	micropore
siliceous TUD-1	757±20	61	696	1.012	–	6.3	–
Beta-TUD-1 (20%)	730±30	161	564	1.08	0.0672	7.4	0.65
Beta-TUD-1 (40%)	637±15	289	353	1.07	0.0819	9.1	0.65
Beta-TUD-1 (60%)	639±7	377	262	0.97	0.098	9.0	0.65
pure zeolite Beta	601±2	399	199	–	0.1207	–	0.65

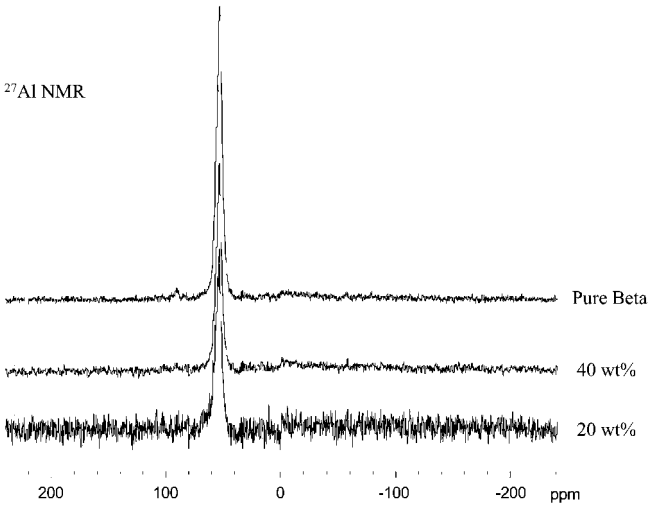

Figure 3. ^{27}Al NMR of pure zeolite Beta and Beta-TUD-1 containing 20 wt% and 40 wt% of zeolite Beta.

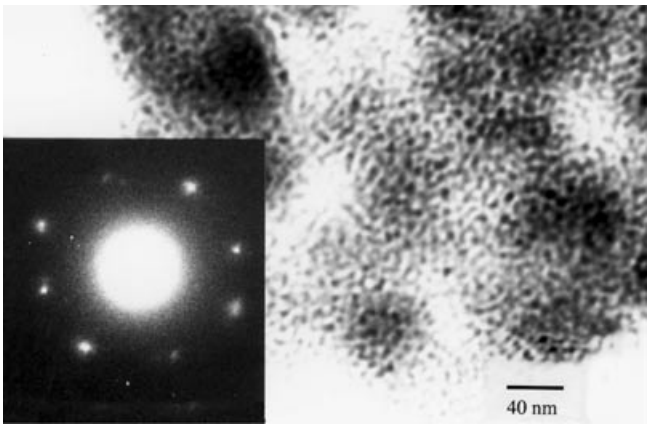

Figure 4. High-resolution transmission electron microscopy (HRTEM) of Beta-TUD-1 with 20 wt% zeolite Beta. Inset: Electronic diffraction pattern of dark gray domains.

Mesoporosity: Figure 5 shows the isotherms of siliceous TUD-1, Beta-TUD-1, and pure zeolite Beta. The adsorption branch of siliceous TUD-1 levels off at a relative pressure of

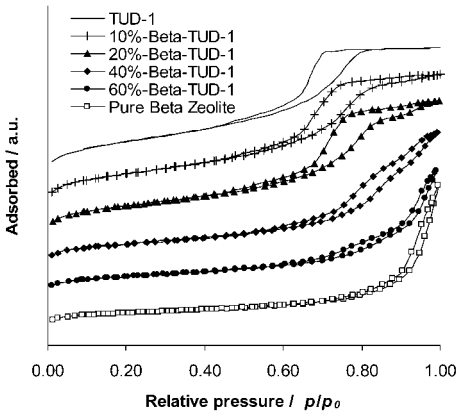

Figure 5. N_2 adsorption–desorption isotherms of Beta-TUD-1 containing different amount of zeolite Beta, pure zeolite Beta, and TUD-1.

0.82 and no more adsorption in the higher relative pressure region occurs, consistent with the absence of textural pores. However, zeolite incorporation changes the isotherms. The amount of adsorption in the higher relative pressure region increases in parallel with the zeolite loading and the isotherms of Beta-TUD-1 gradually shift from siliceous TUD-1 to pure zeolite Beta.

This trend reflects the change of pore size distributions shown in Figure 6. The composites with 10 and 20 wt. % zeolite Beta show only one narrow peak around 5.5 nm and

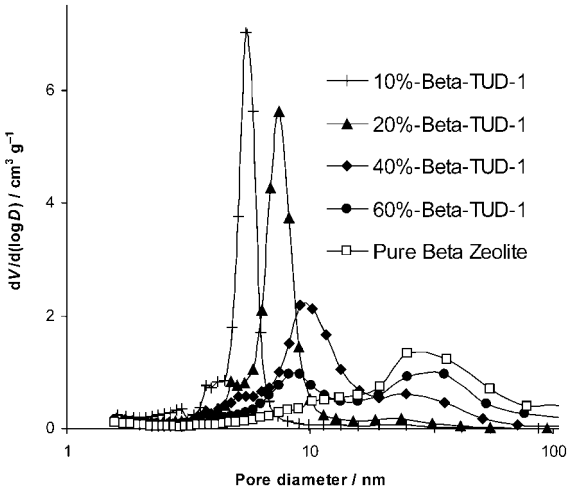

Figure 6. Mesopore size distribution of Beta-TUD-1 containing different amount of zeolite Beta and pure zeolite Beta.

7.5 nm, respectively. However, when the zeolite loading increases to 40 and 60 wt %, a broad peak between 20 and 50 nm occurs and its intensity increases with zeolite loading. An intensive broad peak also appears in the pure zeolite Beta in the same range. It is believed that this broad peak results from interparticle (textural) pores of zeolite, indicating that the zeolite crystals in the mesoporous matrix TUD-1 are not completely isolated when the zeolite loading is 40 wt % or more. Hence, at high loadings some zeolite particles aggregate in the TUD-1 matrix, consistent with the TEM results.

Microporosity: The micropore size distribution plots of Beta-TUD-1 obtained by argon adsorption show peaks consistent with the characteristic pore size of zeolite Beta (cf. Figure 7).

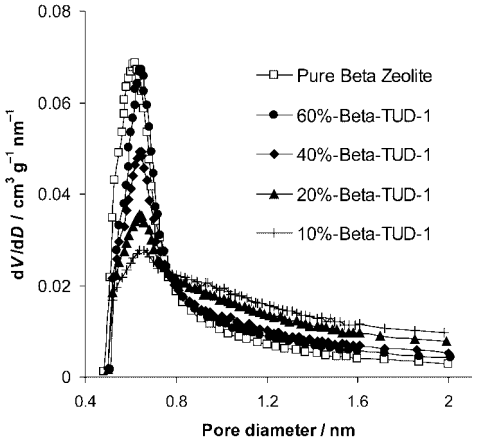

Figure 7. Micropore size distribution of Beta-TUD-1 containing different amounts of zeolite Beta and pure zeolite Beta.

Moreover, the peak areas (reflecting micropore volume) increase with zeolite loading, as expected. The accumulative micropore volumes of zeolite Beta are estimated from the peak area between 5 and 7 Å. Their porosity is summarized in Table 1.

In summary, from the XRD powder patterns, TEM images, gas adsorption, and ^{27}Al NMR spectroscopy, it is concluded that nanosized zeolite Beta is distributed homogeneously throughout the mesoporous matrix of TUD-1. The zeolite particles are completely isolated from each other for up to 20 % zeolite loading. The zeolite crystals are highly accessible through the three-dimensional mesopore structure surrounding the crystals.

Modified acidity: Although the incorporation of zeolite Beta into the mesoporous silica TUD-1 may lead to composite materials in which the dispersion of small (not agglomerated) zeolite particles leads to active sites that are more easily accessible to the reactants, (thereby increasing the catalytic activity), TUD-1 may also cover a fraction of zeolite particles and partially inhibit specific active sites. Additionally, the interaction between TUD-1, which basically consists of an amorphous silica network, and the zeolite Beta crystals may modify the number and strength of acid sites, especially at the interface between the amorphous TUD-1 and the crystalline zeolite particles. Therefore, the overall performance of these composite acid catalysts depends on

which of these effects is dominant. Information concerning the hydroxyl type, distribution, and surface acidity of the composite is mandatory for any understanding that goes beyond descriptive reporting.

The acidity of the composites, along with that of the pure silica TUD-1 and zeolite Beta, has been monitored by FTIR spectroscopy during both CO and NH_3 adsorption at liquid nitrogen and room temperature, respectively. Figure 8 shows the FTIR spectra of the materials before (left panel) and after (right panel) the CO adsorption at 77 K (only the maximum coverage of CO is reported in the figure for sake of clarity).

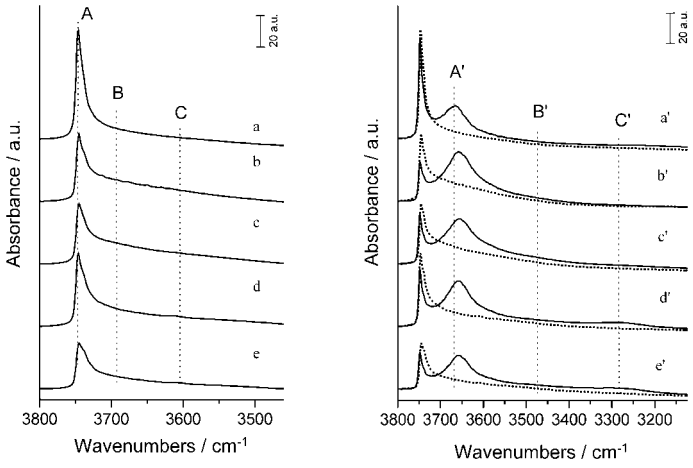

Figure 8. FTIR spectra before (left panel) and after (right panel) CO adsorption at liquid nitrogen temperature: a) TUD-1; b) 20% Beta-TUD-1 composite; c) 40% Beta-TUD-1 composite; d) 60% Beta-TUD-1 composite; e) zeolite Beta; a′–e′) spectra are obtained after admission of 20 Torr CO. The spectra of the bare samples before CO adsorption are also reported in the right panel (dotted lines) for comparison.

As far as the pure TUD-1 sample is concerned (curve a), the spectrum is dominated by an intense band at 3750–3745 cm^{-1}, which is due to the OH stretching of isolated silanols (structure **A**). However, this band shows an asymmetric

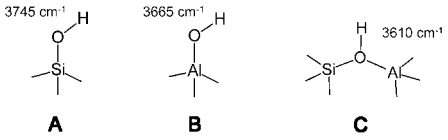

shape along with a large tail extending down to 3600 cm^{-1}; these spectroscopic features suggest that, beside isolated silanols, different families of OH groups absorbing at wavenumbers in very close vicinity are also present in TUD-1: weakly interacting terminal silanols (3740–3725 cm^{-1}) and hydrogen-bonded silanols (3725–3600 cm^{-1}).[19,20] The 3750–3745 cm-1 band becomes less intense and broader in the case of both composites (Figure 8, curves b–d) and of pure zeolite Beta (curve e). This suggests that the presence of hydrogen-bonded silanols is more relevant in these materials. Beside isolated and vicinal silanols, two types of Brønsted acid sites are found in the composites: 1) hydroxyl groups linked to partially extra-framework aluminum ions (structure **B**) that absorb at 3660–3670 cm^{-1} ;[21,22] 2) bridged hydroxyl groups (structure **C**)[21–24] at around 3620–3580 cm^{-1} that are the sites of the strong Brønsted acidity in zeolites.

However, the large band of hydrogen-bonded silanols (Scheme 1), which covers the whole 3725–3600 cm^{-1} range, heavily overlaps with the absorption of the Brønsted hydroxyl groups and makes these bands difficult to detect. In such a case CO adsorption at liquid nitrogen temperature becomes an essential tool to monitor the presence of different hydroxyl groups, as they vibrate with a lower frequencies upon CO adsorption; the downward shift depends on their protonic acidity, thus making the OH absorption more separated and detectable.[22,24] This effect is clearly visible in Figure 8 (right panel), where three different families of hydrogen-bonded hydroxyl groups are found (structures **A**′, **B**′, and **C**′).

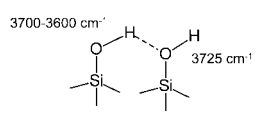

Scheme 1.

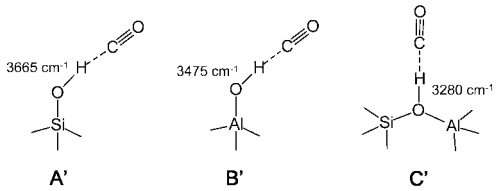

Although the intensity of the bands of the Brønsted OH is very low and broad, clear-cut evidence of the presence of the **B**′ and **C**′ species could be found in carefully designed CO adsorption–desorption experiments and by plotting difference spectra. An estimation of the acidity as determined by the shift of the OH stretching upon CO adsorption is reported in Table 2.

Table 2. The acidity of the OH groups measured by CO adsorption.

	ν_{OH} [cm^{-1}]	$\nu_{OH\cdots CO}$ [cm^{-1}]	$\Delta\nu_{OH\cdots CO}$ [cm^{-1}]	Acidity
Si–OH	3745	3665	80 ± 5	very low
Al–OH	3665[a]	3475[a]	190 ± 30	medium
Si-O(H)-Al	3610	3280	330 ± 10	strong

[a] Estimated values for the band position cannot be detected with high precision.

The presence of a larger variety of hydroxyl groups in the composites, relative to those in pure TUD-1, becomes clearer upon CO adsorption: the band of hydrogen-bonded silanols gets broader and is shifted to lower wavenumbers. The measure of acidity for these groups, reported in Table 2, has to be considered as an average value. The most relevant information on the Brønsted acidity of the Beta-TUD-1 composite which are obtained from the CO experiments can be summarized as follows:

1) The number of bridged hydroxyl groups (**C**, **C**′ species) and the sites of the strongest acidity progressively de-

crease with a decrease in zeolite loading, that is, from the 60% to the 20% composite sample.
2) The 40% sample has the highest concentration of partially extraframework Al-OH groups with medium acidity.

NH_3 adsorption on purely siliceous TUD-1 led to the formation of only weakly bonded Si–OH···NH_3 complexes that could be decomposed simply by evacuation at room temperature similarly to what has been observed for other mesoporous silicas.[20,24] Beside these weak complexes, NH_4^+ ions were formed on the composites. The typical NH_4^+ deformation mode[25] (at around 1460 cm^{-1}) was detected after NH_3 adsorption on all samples with increasing intensity as a function of the zeolite loading (Figure 9). As both medium and

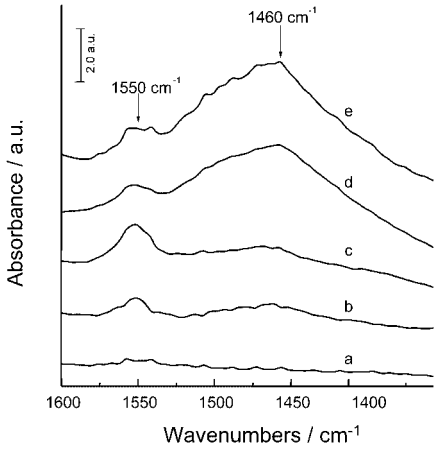

Figure 9. FTIR spectra in vacuum at room temperature after NH_3 adsorption: a) TUD-1; b) 20% Beta-TUD-1; c) 40% Beta-TUD-1; d) 60% Beta-TUD-1; e) zeolite Beta.

strong acid sites are responsible for the formation of ammonium ions, they cannot be distinguished using this approach. However, NH_3 adsorption can be used to monitor the presence of distorted reactive siloxane bridges formed by condensation of two vicinal silanols (Scheme 2, first reaction)

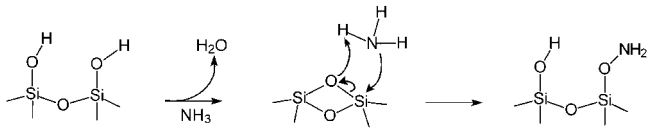

Scheme 2.

on the silica surface during activation processes at temperatures > 500°C. These surface species may play an important role during a catalytic reaction as they easily break in the presence of adsorbates/reactants. Si-NH_2 groups are, for instance, formed by reaction with NH_3 (Scheme 2, second reaction) and, as detected by the NH_2 bending mode at 1550 cm^{-1}, are much more abundant on the 40% sample (Figure 9c).

It is worth noting that the sample that has the highest catalytic activity in cracking reactions shows also the most abundant presence of both Brønsted sites with medium acidity and of distorted siloxane surface bridges. These sites might have a synergistic effect during the cracking reaction in the formation/stabilization of the carbo-cationic intermediates.

Catalytic test: The catalytic activity of Beta-TUD-1 with different loadings has been tested by using *n*-hexane cracking as a model reaction. Figure 10 shows that there is an opti-

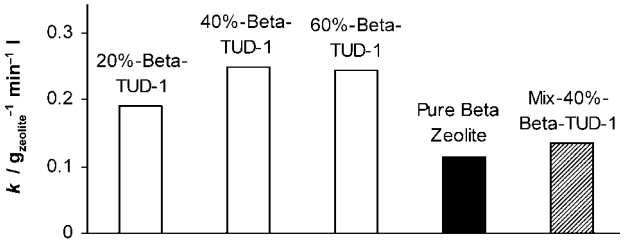

Figure 10. Pseudo-first-order reaction rate constants based on the mass of zeolite for *n*-hexane cracking at 538°C on zeolite Beta-TUD-1 catalysts, the pure zeolite Beta, and a physical mixture of 40 wt% zeolite and TUD-1.

mum zeolite loading in the mesoporous matrix with respect to the catalytic activity of *n*-hexane cracking. The Beta-TUD-1 with 40 wt% zeolite has the highest activity compared to that of 20 and 60 wt%, and about two times higher activity than both the pure zeolite Beta and the physical mixture of 40 wt% zeolite and TUD-1, clearly illustrating the synergy present in the composite.

Two effects might be responsible individually or concurrently for this difference in activity:

1) Nanosized zeolite particles form aggregates in the case of pure zeolite Beta, which reduces the accessibility to zeolite particles buried inside these aggregates. In the composite, the nanosized zeolite particles are surrounded by the mesoporous matrix, which offers high accessibility to almost all zeolite particles. The sample with 20 wt% zeolite shows isolated zeolite particles homogeneously dispersed in the mesoporous matrix. As the zeolite loading increases, nanosized zeolite particles start to aggregate, such that the external surface of zeolite particles covered by the silica matrix is reduced on average, leading the increase of the accessibility to zeolite. However, further increase of the zeolite loading (e.g., 60 wt%) leads to more severe aggregation (confirmed by TEM and gas adsorption), resulting in zeolite particles inside the aggregates with low accessibility. In the case of 40 wt% zeolite loading, TEM showed some very small aggregates, consistent with the composite having neither too much transfer limitation imposed by zeolite particle aggregation nor not too much external surface coverage by the mesoporous silica wall.
2) In addition, the activity is influenced by the chemical interaction between zeolite and matrix, which changes the nature of catalytically active acid sites as outlined above. The presence and functionality of the strained siloxane

2-rings being one of the principle discoveries reported in this paper.

Experimental Section

Materials: Triethanolamine (TEA, 97%) and tetraethylorthosilicate (TEOS, 98%) from ACROS, tetraethylamonium hydroxide (TEAOH, 35%) from Aldrich, and demineralized water were used. zeolite Beta with a Al/Si mole ratio of 150 and a crystal size of around 40 nm (measured with TEM) was supplied by Zeolyst International.

Synthesis: Zeolite particles were homogeneously dispersed in ammonia containing water in a mass ratio of about 1/10~20. A mixture of tetraethylorthosilicate (TEOS) and triethanolamine (TEA) was added to the suspension whilst stirring. After stirring for about 2 h, tetraethylamonium hydroxide (TEAOH) was added dropwise, whilst continuing to stir until gelation of the synthesis mixture occurred. A typical final synthesis gel has a molar composition of TEOS/0.5 TEA/0.1 TEAOH/11 H_2O, excluding the amount of zeolite (about 10–60 wt% zeolite in the final calcined composite). Following the synthesis procedure of TUD-1,[10] the solid gel was aged at room temperature for 6–24 h and dried at 98–100 °C in air for 10 h. After the hydrothermal treatment at 170 °C for 4 h, the composite material was calcined in air for 10 h at 600 °C, using a ramp rate of 1 °C min^{-1}.

Characterization: X-ray powder diffraction (XRD) patterns were recorded with $Cu_{K\alpha}$ radiation on a Philips PW 1840 diffractometer equipped with a graphite monochromator. The samples were scanned in a range of 0.1–40° in 2θ with a step of 0.02°. The presence of mesostructure was confirmed by the low angle (001) reflection peak in between 0.5 and 2° in 2θ.

Microporosity and mesoporosity were determined by argon and nitrogen ad-/desorption measurements, respectively. Argon adsorption isotherms were recorded on a Micrometrics ASAP 2010 at 87 K. Nitrogen ad-/desorption isotherms were measured on a Quantachrome Autosorb-6B at 77 K. Before the measurements, all samples were degassed at 350 °C for 16 h. Micropore and mesopore sizes were calculated from desorption branch using the Saito–Saito–Foley and BJH models, respectively.

High-resolution transmission electron microscopy (HRTEM) was performed on a Jeol JEM-2010 electron microscope operated at 200 kV. Solid-state NMR spectroscopy of ^{27}Al NMR was recorded on a Varian-400 s spectrometer.

FTIR spectra of pellets of the samples were recorded with a Bruker Equinox 55 spectrometer at a resolution of 4 cm^{-1}. NH_3 and CO dosing was performed on template-free samples after thermal treatments under vacuum at 550 °C in suitable IR cells, allowing either room temperature or liquid nitrogen temperature in situ measurements. The spectra are presented in absorbance scale after normalization with respect to the pellet weight.

Catalytic test: The cracking of *n*-hexane was carried out on a fixed catalyst bed of a continuously operated gas flow apparatus at atmospheric pressure and with an *n*-hexane concentration of 6.6 mol% in nitrogen. About 1 g of the catalysts, with a particle size of 125–250 μm, obtained by crushing and sieving, was used in the reactor. As reference catalysts, the pure zeolite Beta and a physical mixture of 40 wt% zeolite Beta and silica TUD-1 was made into pellets (Pressure 200 kg cm^{-2}) and crushed to get the same particle size of 125–250 μm. The physical mixture was obtained by mixing the zeolite and TUD-1, particle size smaller 125 μm, with water followed by evaporation. For activation, the catalyst samples were heated in an airflow of 50 mL min^{-1} from room temperature to 600 °C with a heating rate of 10 °C min^{-1} and kept there for 8 h. The cracking reaction of *n*-hexane was carried out at atmospheric pressure with an *n*-hexane concentration of 6.6 mol% in nitrogen. The reaction temperatures were increased in steps of 10 °C and the modified contact-time based on the mass of catalyst was kept constant. The reaction products were automatically sampled and analyzed with an online gas chromatograph (GC) Chrompack 9000 with flame ionization detector (FID). The GC column used to separate the light cracking products was a 60 m fused silica capillary with an internal diameter of 0.32 mm and a nonpolar bonded phase of dimethylpolysiloxane (film thickness 5 μm). To quantify the catalyst activities, the first-order reaction rate constants for 538 °C were calculated by applying the Arrhenius equation for the reaction temperatures (500, 510, 520, and 530 °C) measured.

Acknowledgement

We thank ABB Lummus Global Inc. for financial support. Thanks to Mr. Johan Groen for gas adsortion and Mr. Arvind Ramachandra for his help in both the synthesis and catalytic testing.

[1] P. B. Weisz, *CHEMTECH* **1973**, *3*, 498–505.
[2] a) M. Yamamura, K. Chaki, T. Wakatusuki, H. Okado, K. Ffujimoto, *Zeolites* **1994**, *14*, 643–649; b) A. J. H. P van der Pol, A. J. Verduyn, J. H. C van Hooff, *Appl. Catal. A* **1992**, *92*, 113–130; c) M. A. Camblor, A. Corma, A. Martinez, F. A. Mocholi, J. P. Pariente, *Appl. Catal.* **1989**, *55*, 65–74.
[3] M. V. Landau, N. Zaharur, M. Herskowitz, *Appl. Catal. A* **1994**, *115*, L7–L14.
[4] C. Madsen, C. J. H. Jacobsen, *Chem. Commun.* **1999**, *8*, 673–674.
[5] a) B. T. Holland, L. Abrams, A. Stein, *J. Am. Chem. Soc.* **1999**, *121*, 4308–4309; b) L. M. Huang, Z. B. Wang, J. Y. Sun, L. Miao, Q. Z. Li, Y. S. Yan, D. Y. Zhao, *J. Am. Chem. Soc.* **2000**, *122*, 3530–3531.
[6] N. van der Puil, Ph.D. Thesis, Delft University of Technology, **1997**.
[7] Kresge CT, M. E. Leonowicz, W. J. Roth, J. C. Vartuli, J. S. Beck, *Nature* **1992**, *359*, 710–712.
[8] S. A. Bagshaw, E. Prouzet, T. J. Pinnavaia, *Science* **1995**, *269*, 1242–1244.
[9] D. Y. Zhao, J. L. Feng, Q. S. Huo, N. Melosh, G. H. Fredrickson, B. F. Chmelka, G. D. Stucky, *Science* **1998**, *279*, 548–552.
[10] J. C. Jansen, Z. Shan, L. Marchese, W. Zhou, N. van der Puil, T. Maschmeyer, *Chem. Commun.* **2001**, *8*, 713–714.
[11] K. R. Kloetstra, H. van Bekkum, J. C. Jansen, *Chem. Commun.* **1997**, *23*, 2281- 2282.
[12] L. M. Huang, W. P. Guo, P. Deng, Z. Y. Xue, Q. Z. Li, *J. Phys. Chem. B* **2000**, *104*, 2817–2823.
[13] Z. T. Zhang, Y. Han, L. Zhu, R. W. Wang, Y. Yu, S. L. Qiu, D. Y. Zhao, F. S. Xiao, *Angew. Chem.* **2001**, *113*, 1298–1301; *Angew. Chem. Int. Ed.* **2001**, *40*, 1258–1262.
[14] Y. Liu, W. Z. Zhang, T. J. Pinnavaia, *Angew. Chem.* **2001**, *113*, 1295–1298; *Angew. Chem. Int. Ed.* **2001**, *40*, 1255–1258.
[15] W. P. Guo, L. M. Huang, P. Deng, Z. Y. Xue, Q. Z. Li, *Microporous Mesoporous Mater.* **2001**, *44*, 427–434.
[16] M. J. Verhoef, P. J. Kooyman, J. C. van der Waal, M. S. Rigutto, J. A. Peters, H. van Bekkum, *Chem. Mater.* **2001**, *13*, 683–687.
[17] C. J. Brinker, G. W. Scherer, *Sol–Gel Science: The Physics and Chemistry of Sol–Gel Processing*, Academic Press, Boston, **1990**.
[18] P. Prokesova, S. Mintova, J. Cejka, T. Bein, *Microporous Mesoporous Mater.* **2003**, *64*, 165–174.
[19] A. Zecchina, S. Bordiga, G. Spoto, L. Marchese, G. Petrini, G. Leofanti, M. Padovan, *J. Phys. Chem.* **1992**, *96*, 4985.
[20] E. Gianotti, V. Dellarocca, L. Marchese, G. Martra, S. Coluccia, T. Maschmeyer, *Phys. Chem. Chem. Phys.* **2002**, *4*, 6109–6115.
[21] A. Zecchina, S. Bordiga, G. Spoto and D. Scarano, *J. Chem. Soc. Faraday Trans.* **1992**, *88*, 2959–2969.
[22] B. Onida, L. Borello, B. Bonelli, F. Geobaldo, E. Garrone, *J. Catal.* **2003**, *214*, 191–199.
[23] S. Kotrel, J. H. Lunsford, H. Knözinger, *J. Phys. Chem. B* **2001**, *105*, 3917–3921.
[24] S. Coluccia, L. Marchese, G. Martra, *Microporous Mesoporous Mater.* **1999**, *30*, 43–56.
[25] A. Zecchina, L. Marchese, S. Bordiga, C. Pazè, and E. Gianotti, *J. Phys. Chem. B* **1997**, *101*, 10128–10135.

Received: April 7, 2004
Published online: August 30, 2004